



Research Report

## Controlled Synthesis and Characterization of Monodisperse CeO<sub>2</sub> Nanostructures

Haruo Imagawa, Akihiko Suda, Kae Yamamura and Shouheng Sun

Report received on Mar. 5, 2014

**■ABSTRACT■** Controlled synthesis of monodisperse CeO<sub>2</sub> nanostructures using thermal decomposition methods in organic solvents with surfactants was investigated. The sizes and shapes of the monodisperse CeO<sub>2</sub> nanoparticles (NPs) were controlled by reaction solvents (1-octadecene or diphenyl ether), and the molar ratio of the Ce-precursor ((NH<sub>4</sub>)<sub>2</sub>Ce(NO<sub>3</sub>)<sub>6</sub>) and surfactants (oleylamine and/or oleic acid) in the reaction mixture. The CeO<sub>2</sub> NPs dispersed on  $\gamma$ -Al<sub>2</sub>O<sub>3</sub> samples were active for oxygen storage and release relative to the physical mixture of aggregated CeO<sub>2</sub> and Al<sub>2</sub>O<sub>3</sub>; smaller NPs show enhanced oxygen storage capacity. Monodisperse CeO<sub>2</sub> nanoplates composed of assembled CeO<sub>2</sub> NPs (ca. 2 nm) were also synthesized by thermal decomposition using a bottom-up approach. Surfactant conditions sensitively affect nanoplate formation of NP assembled structures, based on the decrease in the surface energy of the NPs. X-ray diffraction patterns and transmission electron microscopy indicated selective (200) growth of fluorite cubic CeO<sub>2</sub>. The bandgap energy of CeO<sub>2</sub> nanoplates for direct transitions was larger than that for bulk CeO<sub>2</sub> and monodisperse 6 nm CeO<sub>2</sub> NPs.

**■KEYWORDS■** CeO<sub>2</sub>, Monodisperse, Nanoparticles, Nanoplates, Thermal Decomposition, Bottom-up Approach, Surfactants, Oxygen Storage Capacity, Band Gap Energy

### 1. Introduction

Controlled synthesis for uniform size and shape of monodisperse nanostructures such as nanoparticles (NPs) is a preferable approach for practical applications due to their unique physical properties and morphology. Various nanostructures have been known to form, especially in the presence of surfactants<sup>(1,2)</sup> that inhibit crystal growth of specific planes in the nanostructures, due to their selective attachment to the surface during ripening. Those unique structures have also been obtained by the assembly of small NPs using a bottom-up approach,<sup>(3,4)</sup> where small NPs function as building blocks to provide uniform nanostructures.

Cerium(IV) dioxide (CeO<sub>2</sub>) is an important material for catalytic applications due to the combination of its oxygen vacancy and the Ce<sup>4+</sup>/Ce<sup>3+</sup> redox cycle. For example, the oxygen storage and release properties of the nanostructured ceria are often applied to the three way catalyst in automobile exhaust systems for the best catalytic performance among noble metal catalysts.<sup>(5)</sup> As other interesting catalytic applications of CeO<sub>2</sub>-based materials, low temperature oxidation for CO<sup>(6)</sup> or soot,<sup>(7)</sup> and electrochemical oxidation for methanol<sup>(8)</sup> have been investigated. Ultraviolet (UV)

light protection for window glass and use as an additive in cosmetics with CeO<sub>2</sub> as the UV absorbent<sup>(9)</sup> due to its bandgap energy of ca. 3.2 eV are also well-known applications. In particular, monodisperse CeO<sub>2</sub> NPs has been reported to be useful for selective shielding against harmful UV-B/-C ranges < 310 nm.<sup>(10-12)</sup>

One of the desirable methods for superior performance in such applications is to control the nanoscale size and morphology of CeO<sub>2</sub>. This has led to recent advances in the syntheses of nanostructured CeO<sub>2</sub> with sub-10 nm sizes via hydrothermal,<sup>(13-17)</sup> microemulsion,<sup>(18,19)</sup> and organic phase methods.<sup>(11,12,20,21)</sup> Especially in organic phase methods, thermal decomposition of metal salts with suitable surfactants is known to be a useful method for the formation of monodisperse metal oxide nanostructures with homogeneous size distribution and consistent morphology in a highly dispersed state.<sup>(11,21-24)</sup> Metal oxide nanostructures are formed effectively from chelated nuclei with surfactants such as carboxylic acids and/or amines in high-boiling point organic solvents. With respect to morphology control of monodisperse CeO<sub>2</sub> nanostructures, NP formation has been often reported; however, the facile synthesis of unique structures such as nanorods,<sup>(4,24-26)</sup>

nanowires,<sup>(21)</sup> nanosheets<sup>(27)</sup> and nanoplates<sup>(23,24,28)</sup> with selective plane growth is also a challenge from a research perspective. As the next stage, investigation of specific properties derived from highly dispersed CeO<sub>2</sub> nanostructures is required for future applications.

In this review, the controlled synthesis of monodisperse CeO<sub>2</sub> nanostructures in an organic solvent system by a thermal decomposition method and elucidation of their specific properties leading to future applications are overviewed based on our current research. In section 2, the synthesis of monodisperse CeO<sub>2</sub> NPs and their oxygen storage and release properties are demonstrated.<sup>(26)</sup> In section 3, the synthesis of monodisperse CeO<sub>2</sub> nanoplates based on the assembled NPs using a bottom-up approach are presented for optical properties.<sup>(28)</sup>

## 2. Synthesis of CeO<sub>2</sub> NPs and Their Oxygen Storage and Release Properties<sup>(26)</sup>

### 2.1 Synthesis and Characterization of CeO<sub>2</sub> NPs

Dispersed nanostructured CeO<sub>2</sub> with increased oxygen storage capacity (OSC) is anticipated to become one of the potential catalysts<sup>(29)</sup> for low temperature oxidation or electrochemical oxidation, relative to that using aggregated powder of CeO<sub>2</sub> primary particles. In this section, the facile synthesis of monodisperse CeO<sub>2</sub> NPs, and investigation of their OSC are discussed.

Two different sizes of monodisperse CeO<sub>2</sub> NPs were synthesized by a thermal decomposition method in order to compare their properties. CeO<sub>2</sub> NPs of 4 nm size were prepared by mixing (NH<sub>4</sub>)<sub>2</sub>Ce(NO<sub>3</sub>)<sub>6</sub>, oleylamine (OAm), and oleic acid (OA) in diphenyl ether, and the reaction mixture was heated at 180°C for 2 h. In this synthesis, OAm and OA were added as surfactants with a Ce/OAm/OA mole ratio of 1/3/3. The binding between OA and Ce-ion might facilitate CeO<sub>2</sub> nucleation in diphenyl ether, leading to the formation of smaller CeO<sub>2</sub> NPs.<sup>(22,30)</sup> 6 nm CeO<sub>2</sub> NPs were made by mixing (NH<sub>4</sub>)<sub>2</sub>Ce(NO<sub>3</sub>)<sub>6</sub> and OAm in 1-octadecene, and heating the reaction mixture at 180°C for 2 h. Although only OAm was added as a surfactant in this synthesis with a Ce/OAm molar ratio of 1/6, the total amount of surfactant was kept the same as that in the 4 nm CeO<sub>2</sub> NP synthesis, which may be a key point to obtain CeO<sub>2</sub> NPs with a narrow size distribution. Due to the weak binding of amine to Ce<sup>4+</sup>, CeO<sub>2</sub> nucleation in 1-octadecene might not develop

as early as that in diphenyl ether, which yields larger 6 nm CeO<sub>2</sub> NPs. **Figures 1** (A) and (B) show TEM images of the 4 nm and 6 nm CeO<sub>2</sub> NPs obtained as the final product. The sizes of 35 random NPs measured for the 4 nm and 6 nm CeO<sub>2</sub> NPs were 4.2 nm ± 0.2 nm and 5.8 nm ± 0.6 nm, respectively. HRTEM images (Figs. 1(C) and (D)) clearly revealed that both NPs have a single crystal structure with lattice fringe spacings of 0.32 nm and 0.27 nm representing {111} and {200} planes, respectively, in the fluorite cubic CeO<sub>2</sub> crystal structure.

The amount of OAm was found to play an important role for control of the CeO<sub>2</sub> NPs quality in the reaction mixture. For example, for the 6 nm CeO<sub>2</sub>, a smaller amount of OAm (Ce/OAm = 1/1.5) yielded CeO<sub>2</sub> NPs with irregular shapes and a broad size distribution, as shown in Fig. 1(E). Concerning the effect of the heating temperature, the CeO<sub>2</sub> NPs started to form at a reaction temperature around 150°C (Fig. 1(F)), and then developed into more uniformly sized and shaped NPs during heating at 180 °C. This same tendency was

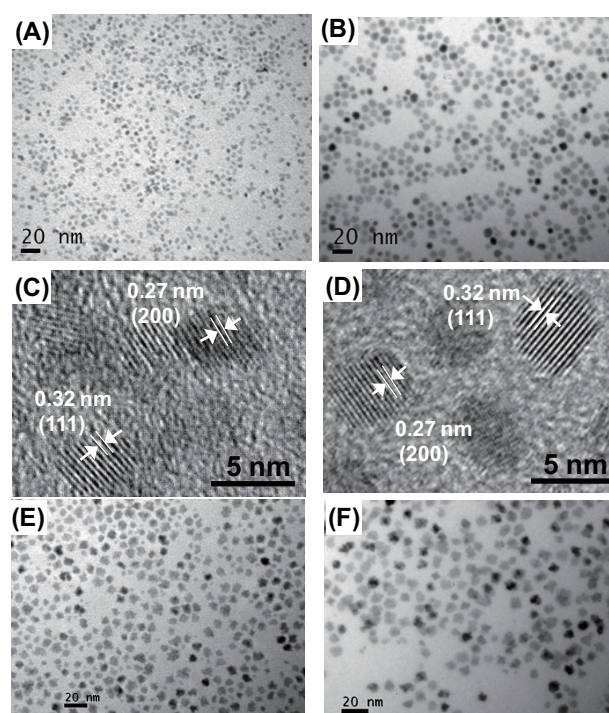


**Fig. 1** TEM images of (A) 4 nm CeO<sub>2</sub> NPs and (B) 6 nm CeO<sub>2</sub> NPs; HRTEM images of (C) 4 nm CeO<sub>2</sub> NPs and (D) 6 nm CeO<sub>2</sub> NPs; TEM images of CeO<sub>2</sub> NPs synthesized in 1-octadecene with a molar ratio of (E) Ce/OAm = 1/1.5 at 180°C and (F) Ce/OAm = 1/6 at 150°C.

observed in the synthesis of 4 nm CeO<sub>2</sub> NPs.

As another type of CeO<sub>2</sub> nanostructure, the synthesis of monodisperse CeO<sub>2</sub> nanorods was also possible by mixing (NH<sub>3</sub>)<sub>2</sub>Ce(NO<sub>3</sub>)<sub>6</sub>, OA and OAm in 1-octadecene (Ce/OAm/OA = 1/3/1.5)<sup>(26)</sup> using the same procedure as for the 6 nm CeO<sub>2</sub> NP synthesis. However, the formation of nanorods is sensitive to surfactant concentration, and they were only formed under the condition of Ce/OA = 1/1.5, not under other OA concentrations. Although the reduced usage of OAm caused CeO<sub>2</sub> NPs to form irregular shapes, as described above, the addition of a small amount of OA in the reaction mixture may help and be effective in consistent nanorod formation.

XRD patterns for 4 nm and 6 nm CeO<sub>2</sub> NP assemblies are shown in **Fig. 2**. Both samples show the typical cubic fluorite (CaF<sub>2</sub>) structure. The average diameters of the 4 nm and 6 nm CeO<sub>2</sub> NPs were 3.7 nm and 5.1 nm, respectively, which were estimated using Scherrer's formula based on the (111) peak at 2θ = 28.5°. These diameters are close to the statistical sizes measured based on the TEM images, as described above.

## 2.2 Preparation of Dispersed CeO<sub>2</sub> NPs on Al<sub>2</sub>O<sub>3</sub>

In order to investigate OSC of the synthesized CeO<sub>2</sub> NPs, the NPs need to be annealed for removal of surfactants from the surface. However, it is necessary to inhibit aggregation of the NPs and allow for sintering in a highly dispersed state during the high temperature annealing treatment at the same time. Therefore, thermally stable γ-Al<sub>2</sub>O<sub>3</sub> (surface area: 135 m<sup>2</sup>/g) was

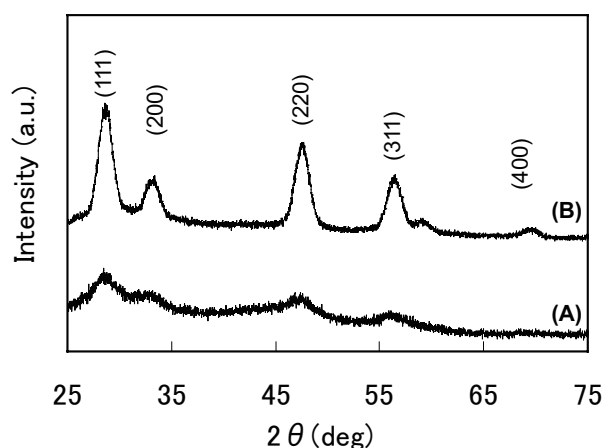


**Fig. 2** XRD patterns for (A) 4 nm CeO<sub>2</sub> NPs and (B) 6 nm CeO<sub>2</sub> NPs.

selected as the support, and NPs were dispersed on a γ-Al<sub>2</sub>O<sub>3</sub> surface.

First, γ-Al<sub>2</sub>O<sub>3</sub> was immersed into an ethanol solution of PVP which was absorbed on the Al<sub>2</sub>O<sub>3</sub><sup>(31)</sup> to ensure that the hydrophobic CeO<sub>2</sub> NPs could be deposited on the hydrophilic γ-Al<sub>2</sub>O<sub>3</sub> surface. Subsequent washing with ethanol removed the extra PVP attached to the γ-Al<sub>2</sub>O<sub>3</sub> surface, giving PVP-Al<sub>2</sub>O<sub>3</sub>. After mixing the hexane dispersion of the CeO<sub>2</sub> NPs and PVP-Al<sub>2</sub>O<sub>3</sub> followed by a hexane wash, the CeO<sub>2</sub> NPs were assembled on the PVP-Al<sub>2</sub>O<sub>3</sub> surface. Annealing at 500°C in air for 30 minutes was sufficient to remove organic species around the NPs, and 15 wt% CeO<sub>2</sub> NPs on Al<sub>2</sub>O<sub>3</sub> samples were formed.

**Figures 3(A)** and **(B)** show TEM images of the 4 nm CeO<sub>2</sub> NPs and 6 nm CeO<sub>2</sub> NPs deposited on γ-Al<sub>2</sub>O<sub>3</sub> after 500°C annealing, respectively. These CeO<sub>2</sub> NPs are well dispersed on the γ-Al<sub>2</sub>O<sub>3</sub> surface without noticeable aggregation or sintering. The structure of the

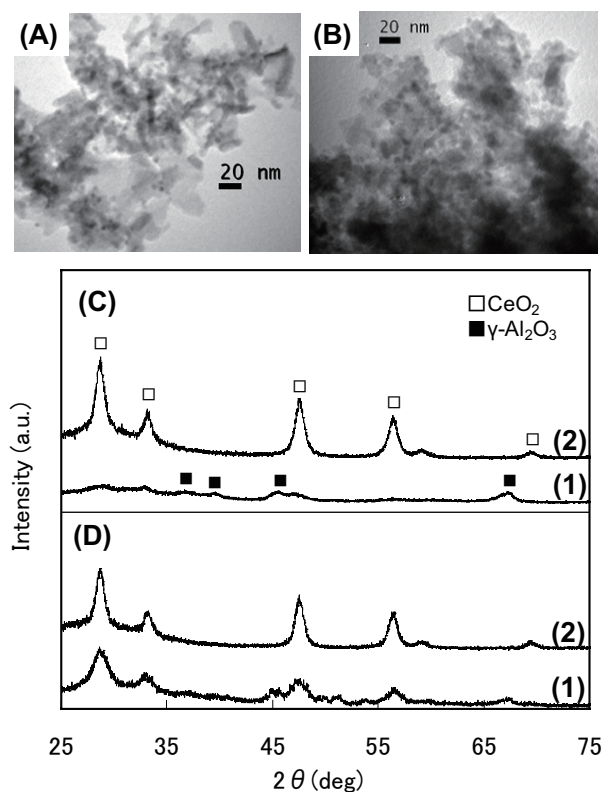


**Fig. 3** TEM images of (A) 4 nm CeO<sub>2</sub> NPs/Al<sub>2</sub>O<sub>3</sub> and (B) 6 nm CeO<sub>2</sub> NPs/Al<sub>2</sub>O<sub>3</sub> after annealing at 500°C. XRD patterns for annealed (C) 4 nm CeO<sub>2</sub> NPs with (1) and without (2) an Al<sub>2</sub>O<sub>3</sub> support, and (D) 6 nm CeO<sub>2</sub> NPs with (1) and without (2) the Al<sub>2</sub>O<sub>3</sub> support.

annealed CeO<sub>2</sub>-Al<sub>2</sub>O<sub>3</sub> samples was further confirmed by XRD (Figs. 3(C)(1) and (D)(1)). The diffraction patterns are the same as those shown in Fig. 2, and the CeO<sub>2</sub> NPs are well stabilized by the  $\gamma$ -Al<sub>2</sub>O<sub>3</sub> support under the annealing condition. On the other hand, CeO<sub>2</sub> NPs without this  $\gamma$ -Al<sub>2</sub>O<sub>3</sub> stabilization grew to ~8 nm size after annealing (Figs. 3(C)(2) and (D)(2)). The stabilization effect of  $\gamma$ -Al<sub>2</sub>O<sub>3</sub> on the CeO<sub>2</sub> NPs was also confirmed by higher temperature annealing at 700 and 1000°C. The average size of the CeO<sub>2</sub> NPs stayed under 20 nm while the NPs in the physical mixture with  $\gamma$ -Al<sub>2</sub>O<sub>3</sub> grew into 50 nm size (Table 1).

### 2.3 Oxygen Storage and Release Properties of CeO<sub>2</sub> NPs

The OSC of the 4 nm and 6 nm CeO<sub>2</sub> NPs supported on  $\gamma$ -Al<sub>2</sub>O<sub>3</sub> was investigated at 500°C, and a physical mix of the aggregated 8 nm CeO<sub>2</sub> NPs and  $\gamma$ -Al<sub>2</sub>O<sub>3</sub> was used as a reference sample. The aggregated 8 nm CeO<sub>2</sub> NPs of the physical mixed sample was obtained after annealing of the 4 nm CeO<sub>2</sub> NPs at 500°C in air.<sup>(26)</sup> For the OSC measurement, all samples were exposed to an oxidative atmosphere (O<sub>2</sub>/N<sub>2</sub>) and a reductive atmosphere (H<sub>2</sub>/N<sub>2</sub>) alternately every 10 min for oxygen storage (O<sub>2</sub> association with CeO<sub>2</sub>) and release (O<sup>2-</sup> dissociation from CeO<sub>2</sub>) tests.<sup>(32)</sup>

The weight changes of these samples during the tests are normalized and given in Table 1. The data clearly reveal that the CeO<sub>2</sub> NP/Al<sub>2</sub>O<sub>3</sub> samples can absorb and release more oxygen than the reference sample. In addition, the smaller CeO<sub>2</sub> NPs (4 nm) showed a larger OSC than the 6 nm CeO<sub>2</sub> NPs. In order to check

the thermal stability, the OSC of the CeO<sub>2</sub> NP/Al<sub>2</sub>O<sub>3</sub> samples annealed at 700°C as an aging test was also measured and shown in Table 1. Although the OSC decreased in all samples according to the increase in the CeO<sub>2</sub> NP size, the 4 nm CeO<sub>2</sub> NPs/Al<sub>2</sub>O<sub>3</sub> sample still had a larger OSC. This is attributed to the larger surface area exposed by the smaller NPs, and further indicates that oxygen molecules involved in the oxygen storage and release process are located mainly on the CeO<sub>2</sub> NP surface.<sup>(33,34)</sup> CeO<sub>2</sub>-based materials on Al<sub>2</sub>O<sub>3</sub> can be stabilized and are effective for inhibition of sintering.<sup>(35)</sup> This trend also contributes to the increased OSC in this dispersed CeO<sub>2</sub> NPs/Al<sub>2</sub>O<sub>3</sub> system.

Pt loading on CeO<sub>2</sub> can enhance both association of O<sub>2</sub> and dissociation of O<sup>2-</sup> on CeO<sub>2</sub>.<sup>(33,36)</sup> The Pt loaded CeO<sub>2</sub>/Al<sub>2</sub>O<sub>3</sub> samples were also prepared, and their OSC was evaluated at 500°C in the same way as in CeO<sub>2</sub>/Al<sub>2</sub>O<sub>3</sub> samples (Table 1). From the OSC data, the addition of Pt was found to enhance the OSC for all samples, and the trend in the OSC is similar to that for the CeO<sub>2</sub>/Al<sub>2</sub>O<sub>3</sub> samples. The data prove that the CeO<sub>2</sub> NPs prepared in this work have great potential as an efficient OSC material for applications not only as automotive catalysts, but also in low temperature oxidation or electrocatalytic oxidation.

## 3. Synthesis of CeO<sub>2</sub> Nanoplates and Their Optical Properties<sup>(28)</sup>

### 3.1 Synthesis and Characterization of CeO<sub>2</sub> Nanoplates

A preferable synthesis method for the formation of

**Table 1** CeO<sub>2</sub> particle size, and OSC of CeO<sub>2</sub>/Al<sub>2</sub>O<sub>3</sub> and Pt/CeO<sub>2</sub>/Al<sub>2</sub>O<sub>3</sub>.

Samples	CeO <sub>2</sub> particle size (nm)			OSC ( $\mu$ mol-O <sub>2</sub> /g sample)		
	500 °C	700°C	1000 °C	As prepared	After aging at 700 °C	Pt loaded
4nm CeO <sub>2</sub> NPs/Al <sub>2</sub> O <sub>3</sub>	3.9	5.8	16.0	65.2	29.2	120.8
6nm CeO <sub>2</sub> NPs/Al <sub>2</sub> O <sub>3</sub>	5.3	6.7	17.7	43.8	20.2	101.6
Physical mix of CeO <sub>2</sub> /Al <sub>2</sub> O <sub>3</sub>	8.0	22.4	50.9	10.0	trace	30.3
Pure CeO <sub>2</sub> *	12.2	15.8	43.5	32.3	4.2	-

\* Comercial CeO<sub>2</sub> without Al<sub>2</sub>O<sub>3</sub>

2D nanostructures such as nanoplates and nanosheets is a bottom-up approach using NPs as building blocks. In this section, the synthesis of monodisperse CeO<sub>2</sub> nanoplates by a bottom-up approach using CeO<sub>2</sub> NPs and their optical properties are discussed.

Monodisperse CeO<sub>2</sub> nanoplates were synthesized by mixing Ce(CH<sub>3</sub>COO)<sub>3</sub>, OA and OAm with a molar ratio of Ce/OAm/OA = 1/1.2/1.2 in 1-octadecene using a thermal decomposition method. The mixture was refluxed at 310°C for 1 h, which is favorable for this synthesis, because nanoplate formation did not reach the threshold at lower reflux temperatures. It is interesting to note that this synthesis is sensitive to conditions of the solvents and precursor salts.<sup>(28)</sup> The shape and monodispersity of the CeO<sub>2</sub> nanoplates were stable and maintained even after an extended reflux time, which indicates that the nanoplates are not an intermediate species for other specific formations.

TEM images reveal 15 nm × 50 nm rectangular CeO<sub>2</sub> nanoplates formed in a monodisperse state (Fig. 4(A)). The CeO<sub>2</sub> nanoplates formed self-assembled nanoarrays, showing their long side surfaces (Fig. 4(B)) or short side surfaces. The width of the side surface is ca. 2 nm, and measurement of 20 nanoplates gives a statistical length of 51.7 ± 3.2 nm. HRTEM images show that the side surface exhibits {200} lattice fringes with an interplanar distance of 0.27 nm (Fig. 4(C)), which corresponds to the cubic fluorite structure. In the front surface of the nanoplate, as shown in Fig. 4(D), a polycrystalline structure with crystal domains

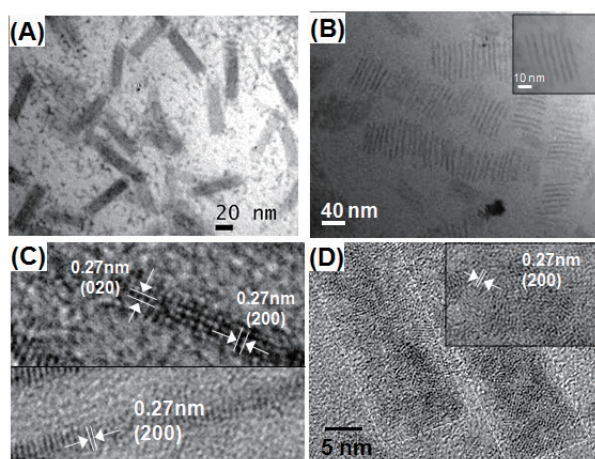


**Fig. 4** TEM images of (A) CeO<sub>2</sub> nanoplates synthesized using 0.3/0.3 mmol of OA/OAm, (B) nanoarray of CeO<sub>2</sub> nanoplates (inset: enlarged image of the side surface of the nanoplates), HRTEM images of the (C) side surface and (D) front surface of the CeO<sub>2</sub> nanoplates.

approximately 2 nm in size was observed by the assembly of small sized NPs as building blocks. These NPs appear to be randomly oriented on the front surface of the nanoplate. Similar randomly oriented polycrystalline domains exhibiting {200} lattice fringes were also observed on the side surfaces.<sup>(28)</sup>

XRD patterns of CeO<sub>2</sub> nanoplates are shown in Fig. 5(A) for confirmation of the crystal structures. The CeO<sub>2</sub> nanoplates were identified as having a cubic fluorite structure and exhibited clear peaks due to (200) and (220) planes, which indicates that selective diffraction occurs on these planes. This result corresponds to the presence of {200} lattice fringes in the HRTEM images of the front and side surfaces of the CeO<sub>2</sub> nanoplates.

### 3.2 Mechanism for Nanoplate Formation

Considering the formation of CeO<sub>2</sub> nanoplates as an assembly of small CeO<sub>2</sub> NPs by a bottom-up approach, the nanoplate formation depends on the amount of surfactants. For example, an excess amount of surfactants did not result in good CeO<sub>2</sub> nanoplate formation. Fig. 6(A) shows the CeO<sub>2</sub> nanostructure formed with a Ce/OAm/OA mole ratio of 1/1.8/1.8, which contained 1.5 times the amount of surfactants than that used in the synthesis of the CeO<sub>2</sub> nanoplates. Smaller CeO<sub>2</sub> nanoplates (ca. 25 nm long) and NPs were observed, but NPs become the dominant species with increased amount of surfactants and the self-assembled nanoplate arrays were rarely observed. A mole ratio of

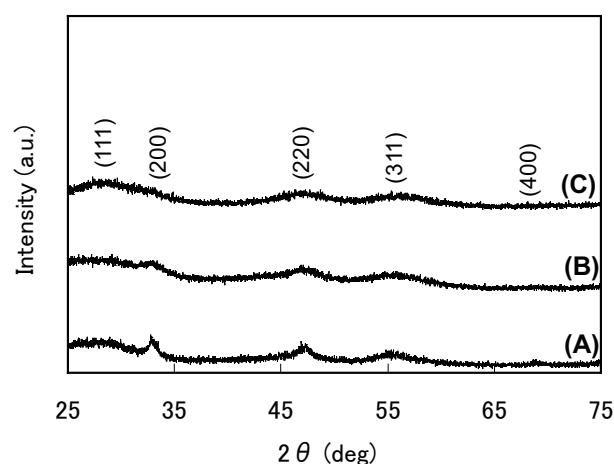


**Fig. 5** XRD patterns for (A) CeO<sub>2</sub> nanoplates synthesized using 0.3/0.3 mmol of OA/OAm, CeO<sub>2</sub> nanostructure synthesized using (B) 0.45/0.45 mmol of OA/OAm, and (C) 0.9/0.9 mmol of OA/OAm.

Ce/OAm/OA = 1/3.6/3.6 resulted in only the formation of CeO<sub>2</sub> NPs (3 nm diameter) (Fig. 6(B)). The CeO<sub>2</sub> NPs show (111) planes. Therefore, a suitable amount of surfactants selectively provides CeO<sub>2</sub> nanoplates as the main product by this bottom-up approach. The XRD results also support the dependence of the surfactant amount on CeO<sub>2</sub> nanoplate formation. The peak growth of (200) and (220) planes is specific to the CeO<sub>2</sub> nanoplate structure as shown in the previous section, but these peaks became indistinct with increasing amount of surfactants (Figs. 5(B) and (C)).

This trend for CeO<sub>2</sub> nanoplate formation can be explained by the following steps. First, 2-nm NPs are synthesized as building blocks and simultaneously assemble to form nanoplates in order to minimize their surface energy, depending on the amount of surfactants present. In the presence of a small amount of surfactants, the dispersity of the CeO<sub>2</sub> NPs is unstable and they tend to assemble to maintain the balance between the amount of surfactants and the surface energy (**Scheme 1(A)**). Therefore, a smaller amount of surfactants tends to preferably yield CeO<sub>2</sub> nanoplate formation.

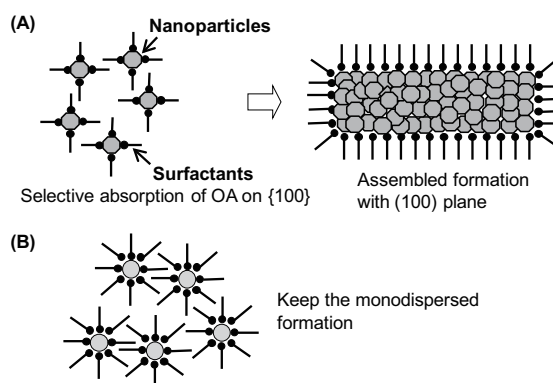
In terms of the selective plane formation, (100) planes in NPs seem to be formed selectively with a small amount of surfactants, probably due to selective adsorption of surfactants on the {100} surface and the subsequent formation of the {100} surface caused by the low growth rate in the [100]. In this step, OA plays an important role in this selective plane formation, because carboxylic groups often stably adsorb on the CeO<sub>2</sub> {100} surface,<sup>(37)</sup> which results in selective (100) plane formation by OA.<sup>(24)</sup> On the other hand, selective crystal growth and assembly do not occur with the addition of a large amount of surfactants, because all facets are randomly covered with excess

surfactants,<sup>(38)</sup> which results in the formation of monodisperse polyhedral CeO<sub>2</sub> NPs as shown above (**Scheme 1(B)**). Thus, the amount of surfactants affects selective crystal growth for specific plane formation during synthesis, which could be exploited to achieve morphology control.

### 3.3 UV Absorption Analysis and Bandgap Energy

CeO<sub>2</sub> has a characteristic absorption in the UV region due to the charge transfer transition from O 2p to Ce 4f. The UV absorption of CeO<sub>2</sub> nanoplates was analyzed and compared with that of the monodisperse 6 nm CeO<sub>2</sub> NPs (**Fig. 7(A)**). Although both samples show absorption around the UV region due to charge transfer, the CeO<sub>2</sub> nanoplate solution exhibits a blue shift of the absorption edge around 400 nm compared with the edge for the 6 nm CeO<sub>2</sub> NP solution.

The bandgap energy of this charge transfer was



**Scheme 1** Schematic illustrations of CeO<sub>2</sub> nanostructure growth under the condition of (A) a small amount of surfactants (nanoplate formation) and (B) a large amount of surfactants (NP formation).

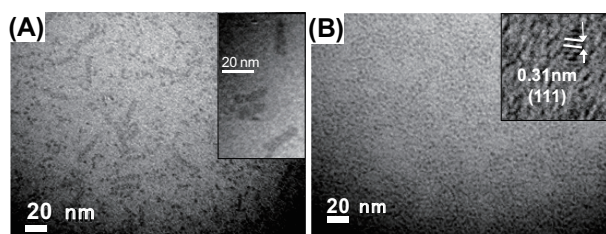


**Fig. 6** TEM images of CeO<sub>2</sub> nanostructures synthesized using (A) 0.45/0.45 mmol of OA/OAm (inset: enlarged image of the nanoplates), and (B) 0.9/0.9 mmol of OA/OAm (inset: HRTEM image of the CeO<sub>2</sub> NPs).

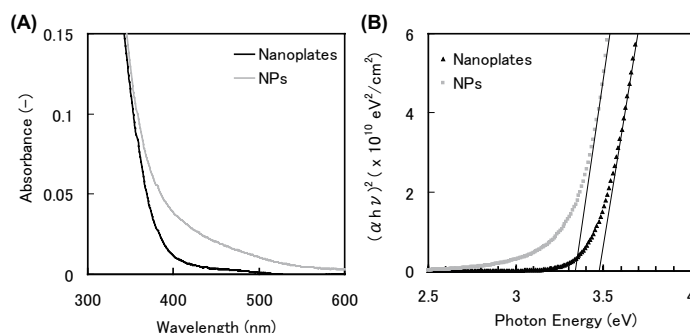


**Fig. 7** (A) UV-vis absorbance spectra, and (B)  $(\alpha h\nu)^2$  as a function of photon energy for CeO<sub>2</sub> nanoplates and 6 nm CeO<sub>2</sub> NPs.

calculated based on the UV-vis spectra, according to the relationship between  $(\alpha h\nu)^2$  and the photon energy (Fig. 7(B)).<sup>(18)</sup> The direct bandgap energy of CeO<sub>2</sub> nanoplates is ca. 3.47 eV, which is larger than that for the 6 nm CeO<sub>2</sub> NPs (3.32 eV). Judging from the bandgap energy of bulk CeO<sub>2</sub> (ca. 3.2 eV),<sup>(26)</sup> both nanostructures have larger bandgap energies than the bulk sample, which is thought to be due to the NP size and the nanosheet thickness, because a quantum size effect has been reported for CeO<sub>2</sub> particles<sup>(11,12)</sup> as seen frequently in TiO<sub>2</sub> nanostructures. Moreover, an increase in the bandgap energy has also been reported for very thin CeO<sub>2</sub> films<sup>(39,40)</sup> and CeO<sub>2</sub> nanosheets,<sup>(27)</sup> regardless of their total surface size with respect to the 2D structure. Therefore, the thickness of the synthesized CeO<sub>2</sub> nanoplates led to the increased bandgap energy, although the value obtained in this experiment is slightly smaller than that in other cases.<sup>(11,27)</sup> This property is promising for applications of the CeO<sub>2</sub> nanoplates for optical or electronic fields such as UV light shielding due to the large bandgap energy.

#### 4. Conclusions

Controlled synthesis of monodisperse CeO<sub>2</sub> nanostructures by thermal decomposition methods in organic solvents with surfactants was investigated. The sizes and shapes of the monodisperse CeO<sub>2</sub> NPs were controlled by adjusting the reaction solvents and the molar ratio of the Ce-precursor and surfactants present in the reaction mixture. The CeO<sub>2</sub> NPs/Al<sub>2</sub>O<sub>3</sub> samples were active for oxygen storage and release, and the smaller NPs showed enhanced OSC.

Monodisperse CeO<sub>2</sub> nanoplates composed of assembled CeO<sub>2</sub> NPs were synthesized by thermal decomposition using a bottom-up approach. The surfactant conditions had a sensitive effect on CeO<sub>2</sub> nanoplate formation of the NP assembled structures, based on the decrease in the surface energy of the NPs. The bandgap energy of the CeO<sub>2</sub> nanoplates for direct transitions was larger than that for monodisperse 6 nm CeO<sub>2</sub> NPs.

These investigations demonstrate that CeO<sub>2</sub> nanostructures obtained from organic phase synthesis are promising for advanced catalytic and optical applications.

#### References

- (1) Qingsheng, L., Yan, Z., Henderson, N. L., Bauer, J. C., Goodman, D. W., Batteas, J. D. and Schaak, R. E., *J. Am. Chem. Soc.*, Vol. 131 (2009), pp. 5720-5721.
- (2) Cao, Y. C., *J. Am. Chem. Soc.*, Vol. 126 (2004), pp. 7456-7457.
- (3) Schliehe, C., Juarez, B. H., Pelletier, M., Jander, S., Greshnykh, D., Nagel, M., Meyer, A., Foerster, S., Kornowski, A., Klinke, C. and Weller, H., *Science*, Vol. 329 (2010), pp. 550-553.
- (4) Kuiry, S. C., Patil, S. D., Deshpande, S. and Seal, S., *J. Phys. Chem. B*, Vol. 109 (2005), pp. 6936-6939.
- (5) Kaspar, J., Fornasiero, P. and Graziani, M., *Catal. Today*, Vol. 50 (1999), pp. 285-298.
- (6) Reddy, B. M., Saikia, P. and Bharali, P., *J. Phys. Chem. C*, Vol. 113 (2009), pp. 2452-2462.
- (7) Katta, L., Sudarsanam, P., Thrumurthulu, G. and Reddy, B. M., *Appl. Catal. B: Environ.*, Vol. 101 (2010), pp. 101-108.
- (8) Lee, E. and Manthiram, A., *J. Phys. Chem. C*, Vol. 114 (2010), pp. 21833-21839.
- (9) Taga, Y., *J. Non-cryst. Solids*, Vol. 218 (1997), pp. 335-341.
- (10) Tsunekawa, S., Fukuda, T. and Kasuya, A., *J. Appl. Phys.*, Vol. 87 (2000), pp. 1318-1321.
- (11) Si, R., Zhang, Y. W., You, L. P. and Yan, C. H., *Angew. Chem., Int. Ed.*, Vol. 44 (2005), pp. 3256-3260.
- (12) Inoue, M., Kimura, M. and Inui, T., *Chem. Commun.* (1999), pp. 957-958.
- (13) Hirano, M., Fukuda, Y., Iwata, H., Hotta, Y. and Inagaki, M., *J. Am. Ceram. Soc.*, Vol. 83 (2000), pp. 1287-1289.
- (14) Mai, H. X., Sun, L. D., Zhang, Y. W., Si, R., Feng, W., Zhang, H. P., Liu, H. C. and Yan, C. H., *J. Phys. Chem. B*, Vol. 109 (2005), pp. 24380-24385.
- (15) Sehgal, A., Lalatonne, Y., Berret, J. F. and Morvan, M., *Langmuir*, Vol. 21 (2005), pp. 9359-9364.
- (16) Yang, S. and Gao, L., *J. Am. Chem. Soc.*, Vol. 128 (2006), pp. 9330-9331.
- (17) Zhang, F., Chan, S. W., Spanier, J. E., Apak, E., Jin, Q., Robinson, R. D. and Herman, I. P., *Appl. Phys. Lett.* (2002), pp. 127-129.
- (18) Masui, T., Fujiwara, K., Machida, K. and Adachi, G., *Chem. Mater.*, Vol. 9 (1997), pp. 2197-2204.
- (19) Bumajdad, A., Zaki, M. I., Eastoe, J. and Pasupulety, L., *Langmuir*, Vol. 20 (2004), pp. 11223-11233.
- (20) Gu, H. and Soucek, M. D., *Chem. Mater.*, Vol. 19 (2007), pp. 1103-1110.
- (21) Yu, T., Joo, J., Park, Y. I. and Hyeon, T., *Angew. Chem., Int. Ed.*, Vol. 44 (2005), pp. 7411-7414.
- (22) Sun, S., *Adv. Mater.*, Vol. 18 (2006), pp. 393-403.
- (23) Wang, D., Kang, Y., Doan-Naguen, V., Chen, J., Kungas, R., Weider, N. L., Bakhmutsky, K., Gorte, R. J. and Murray, R. J., *Angew. Chem., Int. Ed.*, Vol. 50 (2011), pp. 4378-4381.

- (24) Lin, H. L., Wu, C. Y. and Chaing, R. K., *J. Colloid Interface Sci.*, Vol. 341 (2010), pp. 12-17.
- (25) Ahniyaz, A., Sakamoto, Y. and Bergstrom, L., *Cris. Grow. & Design*, Vol. 8 (2008), pp. 1798-1800.
- (26) Imagawa, H., Suda, A., Yamamura, K. and Sun, S., *J. Phys. Chem. C*, Vol. 115 (2011), pp. 1740-1745.
- (27) Yu, T., Lim, B. and Xia, Y., *Angew. Chem., Int. Ed.*, Vol. 49 (2010), pp. 4484-4487.
- (28) Imagawa, H. and Sun, S., *J. Phys. Chem. C*, Vol. 116 (2012), pp. 2761-2765.
- (29) Morikawa, A., Suzuki, T., Kanazawa, T., Kikuta, K., Suda, S. and Shinjoh, H., *Appl. Catal. B: Environ.*, Vol.78 (2008), pp. 210-221.
- (30) Shukla, N., Liu, C., Jones, P. M. and Weller, D., *J. Magn. Magn. Mater.*, Vol. 266 (2003), pp. 178-184.
- (31) Sun, S., Anders, S., Hamann, H. F., Thiele, J. U., Baglin, J. E. E., Thomson, T., Fullerton, E. E., Murray, C. B. and Terris, B. D., *J. Am. Chem. Soc.*, Vol. 124 (2002), pp. 2884-2885.
- (32) Hirano, M. and Suda, A., *J. Am. Ceram. Soc.*, Vol. 86 (2003), pp. 2209-2211.
- (33) Sayle, T. X. T., Parker, S. C. and Sayle, D. C., *Phys. Chem. Chem. Phys.*, Vol. 7 (2005), pp. 2936-2941.
- (34) Kim, S., Merkle, R. and Maier, J., *Surf. Sci.*, Vol. 549 (2004), pp. 196-202.
- (35) Hickey, N., Fornasiero, P., Kaspar, J., Graziani, M., Blanco, G. and Bernal, S., *Chem. Commun.* (2000), pp. 357-358.
- (36) Suda, A., Yamamura, K., Ukyo, Y., Sasaki, T., Sobukawa, H., Tanabe, T., Nagai, Y. and Sugiura, M., *J. Ceram. Soc. Jpn.*, Vol. 112 (2004), pp. 623-627.
- (37) Stubenrauch, J., Brosha, E. and Vohs, J. M., *Catal. Today*, Vol. 28 (1996), pp. 431-441.
- (38) Zhang, J., Ohara, S., Umetsu, M., Naka, T., Hatakeyama, Y. and Adschiri, T., *Adv. Mater.*, Vol.19 (2007), pp. 203-206.
- (39) Sundaram, K. B. and Wahid, P., *Phys. Stat. Sol. B*, Vol. 161 (1990), pp. K63-K66.
- (40) Orel, Z. C. and Orel, B., *Phys. Stat. Sol. B*, Vol. 186 (1994), pp. K33-K36.

Figs. 1-3 and Table 1

Reprinted from *J. Phys. Chem. C*, Vol. 115 (2011), pp. 1740-1745, Imagawa, H., Suda, A., Yamamura, K. and Sun, S., Monodisperse CeO<sub>2</sub> NPs and Their Oxygen Storage and Release Properties, © 2011 ACS, with permission from American Chemical Society.

Figs. 4-7 and Scheme 1

Reprinted from *J. Phys. Chem. C*, Vol. 116 (2012), pp. 2761-2765, Imagawa, H. and Sun, S., Controlled Synthesis of Monodisperse CeO<sub>2</sub> Nanoplates Developed from Assembled Nanoparticles, © 2012 ACS, with permission from American Chemical Society.

Text

Partially reprinted from “The Journal of Physical

Chemistry C, Vol. 115 (2011), pp. 1740-1750” and “The Journal of Physical Chemistry C, Vol. 116 (2012), pp. 2761-2765”, © 2011 and 2012 ACS, with permission from American Chemical Society.

### Haruo Imagawa

Research Fields:

- Nanomaterials Synthesis
- Automotive Catalysts
- Storage Battery

Academic Degree: Ph.D.

Academic Societies:

- American Chemical Society
- Materials Research Society
- Catalysis Society of Japan



### Akihiko Suda

Research Fields:

- Inorganic Synthesis of Colloidal Nanoparticles
- Catalyst Materials
- Porous Oxides

Academic Degree: Dr.Eng.

Academic Societies:

- The American Ceramic Society
- The Ceramic Society of Japan
- The Chemical Society of Japan
- The Society of Powder Technology, Japan

Awards:

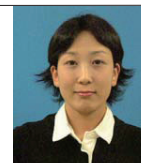
- Technology Prize of the Ceramic Society of Japan, 2003
- Outstanding Paper Award of the Ceramic Society of Japan, 2003
- Chemical Technology Award of the Chemical Society of Japan, 2004
- Environmental Excellence in Transportation Award Runner-up of SAE, 2005



### Kae Yamamura

Research Fields:

- Inorganic Synthesis of Colloids
- Nanopowders
- Catalyst Materials
- Porous Oxides



### Shouheng Sun\*

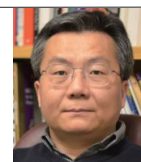
Research Fields:

- Nanomaterials Synthesis
- Self-assembly
- Applications in Nanomedicine, Catalysis, and Energy Storage

Academic Degree: Ph.D.

Academic Societies:

- American Chemical Society
- American Physical Society



\*Brown University